Nuclear Engineering and Design 448 (2026) 114746

Contents lists available at ScienceDirect

Nuclear Engineering and Design

journal homepage: www.elsevier.com/locate/nucengdes

The verification and validation of the coupled neutronics thermal-hydraulics code, MTRDYN, for steady-state condition of RSG-GAS reactor

Surian Pinem [a,*], Farisy Yogatama Sulistyo [a], Peng Hong Liem [b,c], Sukmanto Dibyo [a], Wahid Luthfi [a]

[a] Research Center for Nuclear Reactor Technology, Research Organization for Nuclear Energy, National Research and Innovation Agency, Building 80th KST B.J. Habibie (PUSPIPTEK Serpong), South Tangerang 15310, Banten, Indonesia
[b] Cooperative Major in Nuclear Energy, Graduate School of Engineering, Tokyo City University (TCU), 1-28-1, Tamazutsumi, Setagaya, Tokyo, Japan
[c] Scientific Computational Division, Nippon Advanced Information Service, (NAIS Co., Inc.), 416 Muramatsu, Tokaimura, Ibaraki, Japan

ARTICLE INFO

Keywords:
Neutronic
Thermal hydraulic
RSG-GAS reactor
Steady state
MTRDYN code

ABSTRACT

The in-house coupled thermal-hydraulic and neutronic code, MTRDYN, has been developed with a three-dimensional capability to solve few-group neutron diffusion equations and thermal-hydraulic parameters for plate type fueled research reactor. The multi-group neutron diffusion equations are addressed through neutron flux factorization within an adiabatic kinetic equation. Heat conduction in the fuel element was computed using the finite difference method, with the heat transfer restricted to the radial direction approximation. This study aims to evaluate the accuracy of the MTRDYN in calculating the behavior of RSG-GAS reactor during steady-state operation. The calculated core parameters include excess reactivity, power peaking factor (PPF), fuel cladding temperature, and coolant temperatures. The coolant and cladding temperature obtained from MTRDYN were validated against measured data from instrumented fuel elements (IFE) located at various positions within the core. The calculated excess reactivity for the first and sixth cores differed from experimental results by −160 pcm and 20.0 pcm, respectively. The total control rod reactivity showed a maximum error of 3.9 % compared to experimental results. No significant differences in kinetic parameters were found compared to the RSG-GAS safety analysis report (SAR). The calculated fuel cladding temperatures showed a maximum deviation of 5.78 %. Based on these calculations, the MTRDYN code demonstrates sufficient accuracy in determining the steady-state neutronic and thermal-hydraulic parameters of the RSG-GAS reactor.

1. Introduction

The RSG-GAS reactor reached its first criticality in 1987, becoming the third research reactor constructed in Indonesia. RSG-GAS is a pool-type research reactor utilizing low-enriched uranium oxide fuel (U_3O_8-Al) with 19.75 % enrichment and a density of 2.96 gU/cm^3. In 1999, the U_3O_8-Al fuel was converted to silicide fuel (U_3Si_2-Al) while maintaining the same uranium density (Liem and Sembiring, 2010; Sembiring et al., 2001). RSG-GAS is a multipurpose, high-performance research reactor that operates at a nominal power of 30 MW with an average thermal neutron flux of 2×10^{14} n/cm^{2}s (Pinem and Sembiring, 2019). RSG-GAS features various facilities for neutron beam experiments, irradiation for nuclear fuel and materials, and radioisotope production.

The study of neutronic and thermal-hydraulic parameters plays a crucial role in nuclear reactor safety analysis. Accurate calculation and analysis of neutronic parameters and the fuel cladding temperature distribution are essential for assessing reactor behavior and maintaining safe nuclear reactor operation. Several researchers have developed codes for thermal-hydraulic subchannel calculations in plate-type fuel elements and cladding (Castellanos-Gonzalez et al., 2018; Jo et al., 2014; Kaminaga, 1994), along with various thermal-hydraulic codes to analyze plate-type fuel subchannels (Boustani and Khakshournia, 2020; Iliuk et al., 2016; Vaidya et al., 2010). Most subchannel software codes for plate-type reactors are used to verify specific research reactor parameters.

Software development at BATAN (National Nuclear Energy Agency),

* Corresponding author.
E-mail address: suri001@brin.go.id (S. Pinem).

https://doi.org/10.1016/j.nucengdes.2025.114746
Received 19 August 2025; Received in revised form 31 December 2025; Accepted 31 December 2025
Available online 8 January 2026

now known as part of BRIN (National Research and Innovation Agency), has involved the development of 2-D and 3-D multi-group neutron diffusion codes for plate-type research reactors, namely BATAN-2DIFF (Liem, 1994) and BATAN-3DIFF (Liem, 1999). Additionally, a core fuel management code, BATAN-FUEL (Liem, 1996), was developed and has been routinely applied for core management in the RSG-GAS reactor. The BATAN-FUEL program has been validated against measured neutronic parameters of the RSG-GAS core (Kuntoro et al., 2021; Pinem et al., 2016a). Later, the MTRDYN code was developed as a tool for calculating the safety-related neutronic parameters for the RSG-GAS reactor operation and experiment (Pinem and Sembiring, 2006). The core power distribution from the neutronic solver was then used as the power source for the node-wise subchannel thermal-hydraulic solver in the MTRDYN. Heat conduction in the fuel plate was resolved using the finite difference method, accounting for both time and spatial variations, with the assumption that heat transfer occurs solely in the radial direction. Three-dimensional coupled neutronic and thermal-hydraulic models were solved using spatial discretization by the finite difference method, while the implicit method solved the time function.

Various transient events, including reactivity insertion accident (RIA) analysis, have been studied using the MTRDYN code for the RSG-GAS (Dibyo et al., 2021; Pinem et al., 2022; Pinem et al., 2020a). This study aims to validate the MTRDYN performance in calculating the steady-state neutronic and thermal-hydraulic parameters, including excess reactivity, kinetic parameters, coolant temperature, and fuel-cladding temperature, to compare with the experimental data. Other parameters, such as radial power peaking factor and axial temperature distribution, were compared to the other existing calculation data. Coolant and fuel cladding temperature measurements were obtained using Instrumented Fuel Elements (IFE) RI-10 and IFE RI-11, which were installed at various core positions in the reactor. The cores being evaluated were the first and sixth cores of the RSG-GAS reactor, which correspond to the existing measurement being considered for this study.

2. MTRDYN

2.1. Motive, goals, and challenges

The development of coupled neutronic and thermal-hydraulic (N/TH) code systems originated from the necessity to perform deterministic safety assessments for nuclear power plants (NPPs). A common approach is coupling two pre-existing neutronic codes and a thermal-hydraulic code, sometimes developed independently at national laboratories, for accurately modeling the dynamic response between the two sets of physical properties. This kind of “external coupling” uses a separate process to exchange data between both codes with an external script. Another, more integrated approach is to fully integrate both N/TH solvers with the neutronic and thermal-hydraulic modules are linked into a single code. This approach of “internal coupling” makes it easier for the users to make the input script to model the reactor core and its related system components (Akbas et al., 2015, 2019). Both approaches showed a good performance for simulating the safety-related reactor parameters that are essential either in steady state or transient problems of the reactor system.

External coupling between Monte Carlo (MC) neutron transport codes with Computational Fluid Dynamics (CFD) codes is often used for high-fidelity research and design. It combines the accuracy of a neutronic model being solved using Monte Carlo with the detailed heat transfer (affected by the change in fluid flow) capabilities of CFD (Vazquez et al., 2012). The challenge with this type of coupling is the need for a robust mesh mapping or interpolation scheme between the different meshes used by both neutronic and CFD codes. Since most of the Monte Carlo simulations were developed using a cell structure by CSG (Constructive Solid Geometry) methods, while CFD codes rely on typically finer and often unstructured mesh (Hu and Rizwan-uddin, 2008; Wu and Kozlowski, 2015; Zhang et al., 2021). While some Monte Carlo codes have developed the capabilities to utilize CAD-based geometry, such as MCNP, Serpent, and OpenMC, the coupling mechanism to typical CFD codes and deterministic codes (subchannel code or a reactor core system analysis code, such as RELAP) is still quite challenging since it needs a manual tune-in to consolidate the mesh region or nodes being used between both codes (Cardoni and Rizwan-uddin, 2011; Lago et al., 2024; Leppänen, 2022; Loi et al., 2024; Suikkanen et al., 2014).

The development of large and fast computers, including their accessibility to the users, influenced modern nuclear reactor analysis methods, which enable a significant transition from simplified analytical techniques to a high-fidelity, coupled MC-CFD method as previously mentioned. Simplified analytical techniques or in their numeric approach can be called a deterministic method often sacrificing detailed spatial and temporal parameters (Duderstadt and Hamilton, 1977). The choice between these two methods involves a fundamental trade-off between computational fidelity and cost (running time and hardware specification). Deterministic codes are highly efficient for simulating time-dependent transients due to relying on simplified assumptions such as multigroup energy structures, homogenized cross-sections, and a simple thermal hydraulics approach, such as single-phase sub-channel analysis.(Akbas et al., 2015; Shemon et al., 2014). Monte Carlo codes offer a higher degree of physical fidelity but at a significant computational cost, limiting their use for solving scenarios needed for the Safety Analysis Report (SAR), which is needed in developing reactor design, while their use as a more detailed model as a comparation for deterministic codes might be considered for steady-state problems (Novak et al., 2022; Passons and Tsvetkov, 2022; Stauff et al., 2024; Vazquez et al., 2012).

The numerical methods used to discretize the governing equations in space and time are a critical differentiator between reactor simulation codes. The finite-difference method could be used for spatial discretization, which is a well-developed and robust method for codes with a specific coordinate system (Akbas et al., 2015). Another widely used method for spatial discretization is the Nodal Method, which solves the averaged parameters over large, homogenized regions (nodes), and it has been implemented to our in-house code, the NODAL3, and open source PWR Core Simulator, KOMODO, showing a considerable improvement on calculation time. Other commercial codes, such as PARCS and NESTLE, also use a similar approach, which is computationally efficient and has become the standard for performing full-core, time-dependent analyses in most Light Water Reactor (LWR) safety codes (Alnaqbi et al., 2022; Imron, 2019; Imron and Hartanto, 2021; Osusky et al., 2018; Pinem et al., 2024; Pinem et al., 2025a; Pinem et al., 2016b; Pourrostam et al., 2021; Purdue University, 2004). Another approach, such as Finite-Element Method (FEM), has been used widely through the development of the MOOSE Framework by Idaho National Laboratory and featured at the PROTEUS developed by Argonne National Laboratory (Pater, 2019; Shemon et al., 2014). This method discretizes the spatial domain into a mesh of finite elements to solve the equations, which is compatible with the Griffin module of MOOSE, offering high geometric flexibility, allowing for detailed modeling of complex core components (INL, 2025; Prince et al., 2024).

On the other hand, the choice of integration method for the temporal (time) variable has a direct impact on a code's stability and efficiency for a transient problem. The implicit method solves the variables at the next time step simultaneously with the current time, which provides excellent numerical stability. This stability was advantageous for systems having a widely varying time scales (stiff) as it allows for large time steps (interval), hence reducing overall computational cost for long transients' problems. On the other hand, the explicit methods, which solve the next time step using the current time, require very small time steps to maintain their stability, limiting their practicality for a long transient problem (Akbas et al., 2019; Imron, 2019; Liem et al., 2016).

In the 90s, BATAN was developing various calculation codes by using the best approach can be applied at that time, to calculate the core

safety-related parameter, while utilizing the measured data from the MTR-type reactor commissioned in 1987, RSG-GAS (Operasi Reaktor, 1987; Pinem et al., 2025b). A 2-D diffusion approach was developed in 1994, named BATAN-2DIFF, which was later developed with depletion capability for the RSG-GAS in-core fuel management, later known as BATAN-FUEL (1996) (Liem, 1994, 1996). The next development was to improve the diffusion code to facilitate 3-D Cartesian geometry for a detailed core model, marking the development of our BATAN-3DIFF code (Liem, 1999; Sembiring and Liem, 1999). Then, in the early 2000s, following the similar approach being used, the MTRDYN code was developed by improving BATAN-3DIFF capabilities, adding a hard-coded single-phase subchannel thermal-hydraulic solver to facilitate a coupled neutronic and thermal-hydraulic calculation, adding the dynamic calculation capability to the code. This code was named MTRDYN as the acronym of MTR-type reactor dynamic, which, in the beginning, was able to solve either static or dynamic problems for RSG-GAS (Dibyo et al., 2024; Pinem et al., 2022; Pinem and Sembiring, 2006). Its performance opens its potential for being used in other reactor cores with similar plate-type fuel elements in cartesian geometry (Dibyo et al., 2021; Pinem et al., 2020b).

In the recent period, most of these codes were used as it is, with the code being adequately maintained but not significantly upgraded, due to the limitations on the personnel capabilities and the lack of urgency for adding feature updates. The concern for maintaining knowledge management has arisen within our institution, including maintaining the aforementioned in-house codes developed. With limited computational resources and limited access to other "Gold Standard" codes developed worldwide, the practical approach was to use a fast and reliable deterministic code while also developing personnel capabilities in open-access nuclear codes.

2.2. Neutronic model

The time-dependent neutron diffusion equation for a few energy groups typically expressed as:

$$\frac{1}{v_g}\bullet\frac{\partial\varphi_g(r,t)}{\partial t}=\nabla\bullet D_g(r,t)\bullet\nabla\varphi_g(r,t)-\Sigma_{rg}(r,t)\varphi_g(r,t)+\sum_{g'=1}^{G}\Sigma_{s\,g'\to g}(r,t)\varphi_{g'}(r,t)+\chi_{p\,g}\sum_{g'=1}^{G}\nu_{p\,g'}\Sigma_{f\,g'}(r,t)\varphi_{g'}(r,t)+\sum_{k=1}^{K}\chi_{d\,k\,g}\lambda_k C_k(r,t)\;g=1,\ldots,G \tag{1}$$

while the delayed neutron precursor equation commonly expressed as:

$$\frac{\partial C_k(r,t)}{\partial t}=\sum_{g'=1}^{G}\nu_{d\,k\,g'}\Sigma_{f\,g'}(r,t)\varphi_{g'}(r,t)-\lambda_k C_k(r,t)\;k=1,\ldots,K \tag{2}$$

with (r,t) corresponds to its position and time. While:

v_g, average neutron speed at group g.

$\varphi_g(r,t)$, neutron flux at group g.

$D_g(r,t)$, diffusion coefficient.

$\Sigma_{rg}(r,t)$, macroscopic removal cross section.

$\Sigma_{s\,g'\to g}(r,t)$, macroscopic scattering cross section from group g' to g.

$\nu_{p\,g'}\Sigma_{f\,g'}(r,t)$, prompt neutrons fission cross section, with $\nu_{p\,g'}\approx(1-\beta)\nu_{g'}$

$\chi_{p\,g}$, prompt neutron chi for group g

$\chi_{d\,k\,g}$delayed neutron chi for group g from precursor group k

λ_k, precursor decay constant

$C_k(r,t)$, precursor group k concentration

$\nu_{d\,k\,g'}\Sigma_{f\,g'}(r,t)$, precursor group k production cross section from fission $\nu_{d\,k\,g'}\approx\beta_k\nu_{g'}$

The right-hand side of Eq. (1) enumerates the processes affecting neutron population, with first two terms signify neutron losses attributed to leakage and removal from energy group g. Conversely, neutron production through in-group scattering, prompt fission, and delayed neutron from fission are represented by the third, fourth, and fifth terms, respectively. The right-hand side of Eq. (2) shows precursor dynamics caused by its generation from fission reactions (first term) and its depletion via precursor decay (second term). Both equations explicitly incorporate key nuclear parameters: ν_d and χ_d for delayed neutrons, and ν_p and χ_p for prompt neutron, taking account to the effective delayed neutron fraction β.

MTRDYN adopts a flux factorization approach to facilitate a robust and efficient problem solution. This approach partitions the time-dependent neutron flux into time-dependent amplitude $p(t)$ and shape functions $\Psi_g(r,t)$ shown below

$$\varphi_g(r,t)=p(t)\Psi_g(r,t)\;p(0)=1 \tag{3}$$

The shape function satisfies the following constraint with $\varphi_g^+(r,0)$ represents initial adjoint neutron flux:

$$\frac{\partial}{\partial t}\int\sum_{g=1}^{G}\frac{\varphi_g^+(r,0)\Psi_g(r,t)}{v_g}dV=0 \tag{4}$$

From a physical standpoint, the shape function changes (considerably) slowly over time compared to the amplitude function. This characteristic permits the use of larger time intervals when computing the shape function.

Utilizing Eqs. (3 and 4) in conjunction with the principles of perturbation theory, both Eqs. (1 and 2) can be modified into two equivalent equations, such as the amplitude function:

$$\frac{dp(t)}{dt}=\frac{\rho(t)-\beta(t)}{\Lambda(t)}p(t)+\sum\nolimits_{k=1}^{K}\lambda_k C_k \tag{5}$$

$$\frac{\partial C_k(t)}{\partial t}=\frac{\beta_k(t)}{\Lambda(t)}p(t)-\lambda_k C_k(t)\;k=1,\ldots,K \tag{6}$$

and the shape function as follows.

$$\frac{1}{v_g}\bullet\left(\frac{\partial\varphi_g(r,t)}{\partial t}+\frac{1}{p(t)}\frac{dp(t)}{dt}\Psi_g(r,t)\right)=\nabla\bullet D_g(r,t)\bullet\nabla\Psi_g(r,t)-\Sigma_{rg}(r,t)\Psi_g(r,t)+\sum_{g'=1}^{G}\Sigma_{s\,g'\to g}(r,t)\Psi_{g'}(r,t)+\chi_{p\,g}\sum_{g'=1}^{G}\nu_{p\,g'}\Sigma_{f\,g'}(r,t)\Psi_{g'}(r,t)+\sum_{k=1}^{K}\chi_{d\,k\,g}\lambda_k C_k(r,t)\;g=1,\ldots,G \tag{7}$$

The integral kinetic parameters in Eqs. (5 and 6) are defined as

$$\beta_k(t)\equiv\frac{1}{F(t)}\int\sum\nolimits_{g=1}^{G}\varphi_g^+(r,0)\chi_{dkg}\sum\nolimits_{g'=1}^{G}\nu_{dkg'}\Sigma_{fg'}(r,t)\Psi_{g'}(r,t)dV \tag{8}$$

$$\beta(t)\equiv\sum\nolimits_{k=1}^{K}\beta_k(t) \tag{9}$$

$$\Lambda(t)\equiv\frac{1}{F(t)}\int\sum\nolimits_{g=1}^{G}\varphi_g^+(r,0)\left[\frac{1}{v_g}\right]\Psi_g(r,t)dV \tag{10}$$

$$\rho(t)\equiv-\frac{1}{F(t)}\int\sum\nolimits_{g=1}^{G}\varphi_g^+(r,0)\Delta\Sigma_{rg}(r,t)\Psi_g(r,t)dV+\frac{1}{F(t)}\int\sum\nolimits_{g=1}^{G}\varphi_g^+(r,0)\Delta\left[\sum_{g'=1}^{G}\Sigma_{s\,g'\to g}(r,t)+\chi_{p\,g}\sum_{g'=1}^{G}\nu_{p\,g'}\Sigma_{f\,g'}(r,t)\right]\Psi_{g'}(r,t)dV \tag{11}$$

$$F(t) \equiv \int \sum_{g=1}^{G} \varphi_g^+(r,0)\chi_g \sum_{g'=1}^{G} \nu_{g'}\Sigma_{fg'}(r,t)\Psi_{g'}(r,t)dV \tag{12}$$

with $p(t)$ is the amplitude function, $\beta(t)$ is the total delayed neutron fraction, $\rho(t)$ is net reactivity and $\Lambda(t)$ is prompt neutron generation time.

2.3. Adiabatic model

The Adiabatic Model (AM) implemented in MTRDYN was developed with two key assumptions. First, the energy spectra of prompt and delayed neutrons are assumed to be similar, or the differences are negligible. This means delayed neutrons are treated as if they are emitted from their precursors at the same time as prompt neutrons. Another assumption being considered was that the derivatives of both amplitude and shape functions are assumed to always be zero. Consequently, Eqs. (2–5) simplifies to:

$$\begin{aligned}\nabla D_g(r,t)\cdot\nabla\Psi_g(r,t) - \Sigma_{rg}(r,t)\Psi_g(r,t) + \sum_{g'=1}^{G}\Sigma_{sg'\to g}(r,t)\Psi_{g'}(r,t) \\ + \frac{1}{k_{eff}}\chi_g\sum_{g'=1}^{G}\nu_{g'}\Sigma_{fg'}(r,t)\Psi_{g'}(r,t) = 0\end{aligned} \tag{13}$$

k_{eff} denotes the effective multiplication factor, and the shape function can be determined by applying the eigenvalue criticality procedure. The shape function $\Psi_g(r,t)$ was updated following the update on few-group cross sections for each region, which also update the kinetic parameters through adjoint calculation.

2.4. Thermal-hydraulic model

The thermal-hydraulics module of the MTRDYN was developed for plate-type fuel sub-channels with single-phase coolant flow. The heat conduction equations at fuel plates are solved with a radial-only heat transfer approximation. The single-phase fluid flow was used, with the mass flow rate for each coolant channel from user-defined input, which was assumed to be equal through each coolant channel node near heat-generating regions. The mass continuity and energy conservation equations were then solved with the thermal module of MTRDYN after space discretization using the finite-difference method and implicit method in the temporal domain.

2.4.1. Heat conduction in the fuel plate

The heat conduction equation for the 1D (x-axis) fuel plate can be written as

$$\rho(x,t)C(x,t)\frac{\partial T(x,t)}{\partial t} = \frac{\partial}{\partial x}\,k(x,t)\frac{\partial}{\partial x}T(x,t) + q(x,t) \tag{14}$$

with

$C(x,t)$, fuel meat specific heat
$\rho(x,t)$, fuel meat density
$T(x,t)$, fuel meat temperature
$k(x,t)$, fuel meat thermal conductivity
$q(x,t)$, power density (volumetric power generation)

Eq. (14) was completed by the boundary conditions:

$$-k(x,t)\,\frac{\partial}{\partial x}T\left(x,t\right)\Big|_{x=0} = 0 \tag{15}$$

$$-k(x,t)\frac{\partial}{\partial x}T\left(x,t\right)\Big|_{x=X_F} = q''(X_F,t) \tag{16}$$

$$-k(x,t)\frac{\partial}{\partial x}T\left(x,t\right)\Big|_{x=X_{CL}^{in}} = q''\left(X_{CL}^{in},t\right) = H_g\left[T(X_F,t) - T\left(X_{CL}^{in},t\right)\right] \tag{17}$$

$$-k(x,t)\frac{\partial}{\partial x}T\left(x,t\right)\Big|_{x=X_{CL}^{out}} = q''\left(X_{CL}^{out},t\right) = h\left[T\left(X_{cl}^{out},t\right) - T_L(t)\right] \tag{18}$$

with

X_F, half thickness of the fuel meat
X_{CL}^{in}, distance of the inner cladding
X_{CL}^{out}, distance of the outer cladding
H_g, effective thermal conductance of gap between fuel meat and inner cladding
$q''\left(X_{CL}^{in},t\right)$, heat flux at the inner fuel cladding
$q''(X_F,t)$, heat flux at the fuel meat outer surface
$T_L(t)$, bulk coolant temperature

Although the gap conductance was included in the above equations, in general, there was no gap between the fuel meat and cladding, hence the gap conductance can be neglected. The time-dependent equations are solved by implicit method and the resulting nonlinear equations are linearized taking the values of thermal conductivity k, density ρ and specific heat C from the previous time step. The resulting three-diagonal system of linear equations was then solved by the Gauss Elimination Method. The steady-state form of the heat conduction equations was obtained by setting the $\frac{1}{\Delta t}$ term to zero. The same solution procedure was used in this case.

2.4.2. Fluid dynamics equations of the coolant

The general equations for the coolant temperature distribution in the axial direction with coolant flow only in the Z-axis can be written in the following form:

$$\rho_L(z,t)C_L(z,t)\frac{\partial T_L(z,t)}{\partial t} + G_L(z,t)C_L(z,t)\frac{\partial T_L(z,t)}{\partial z} = \gamma q_L''(z,t) + q_L'''(z,t) \tag{19}$$

with all parameters changes along the fuel plate z-axis, where

$\rho_L(z,t)$, coolant density
$C_L(z,t)$, coolant specific heat
$T_L(z,t)$, bulk coolant temperature
$G_L(z,t)$, coolant mass flow rate
$q_L''(z,t)$, fuel cladding heat flux between the surface and coolant
γ, the surface area of the cladding to the volume of the coolant ratio
$q_L'''(z,t)$, volumetric power density at the coolant

The equations are discretized in the axial direction so they could coincide with the neutronics axial mesh. The z-derivative was approximated as

$$\frac{\partial T_L(z,t)}{\partial z} = \frac{2\left[T_{Li}(t) - T_{Li}^{in}(t)\right]}{\Delta z_i} \tag{20}$$

with i correspond to the axial node, hence $T_{Li}(t)$ is the average coolant temperature, $T_{Li}^{in}(t)$ is the inlet coolant temperature and Δz_i is the axial height of the node. The inlet temperature for the node i was computed using the linear interpolation from the previous node $i-1$ (as)

$$T_{Li}^{in}(t) = 2T_{Li-1}(t) - T_{Li-1}^{in}(t) \tag{21}$$

The resulting equation for the coolant temperature is:

$$\rho_{Li}(t)C_{Li}(t)\frac{\partial T_{Li}(t)}{\partial t} + G_{Li}(t)C_{Li}(t)\frac{2\left(T_{Li}(t) - T_{Li}^{in}(t)\right)}{\Delta z_i} = \gamma\psi_i(t) + q_{Li}(t) \tag{22}$$

Using the fully-implicit scheme, the eq. (3–13) can be written as

$$T_{Li}(t+\Delta t)\left[\rho_{Li}(t+\Delta t)C_{Li}(t+\Delta t)\frac{1}{\Delta t}+G_{Li}(t+\Delta t)C_{Li}(t+\Delta t)\frac{2}{\Delta z_i}\right] = \gamma\psi_i(t+\Delta t)+q_{Li}(t+\Delta t)+T_{Li}(t)\left[\rho_{Li}(t+\Delta t)C_{Li}(t+\Delta t)\frac{1}{\Delta t}\right]+T_{Li}^{in}(t+\Delta t)G_{Li}(t)C_{Li}(t)\frac{2}{\Delta z_i} \quad (23)$$

The nonlinear eq. (23) was linearized using the values of the coolant density ρ_{Li} and the coolant specific heat C_{Li} from the previous time step. A constant mass flow rate, C_{Li}, was then applied to all axial nodes. The cladding surface heat flux was approximated using the cladding and coolant temperatures from the previous time step

$$q''_{Li}(t+\Delta t)\approx h_{Li}(t)\left[T\left(R_{cl}^{out},t\right)-T_{Li}(t)\right] \quad (24)$$

where the heat transfer coefficient $h_i(t)$ is computed using the inlet coolant temperature $T_{Li}^{in}(t+\Delta t)$. To compute the heat transfer coefficient, the Dittus-Boelter correlation was applied:

$$h_{Li}=0.023Re^{0.8}Pr^{0.4}\frac{k_L}{D_e} \quad (25)$$

with k_L is the coolant thermal conductivity, and D_e is the coolant flow channel equivalent hydraulic diameter. The Reynolds (Re) and Prandtl (Pr) numbers are defined as

$$Re=\frac{D_e\,G}{\mu}=\frac{[L]\,[M.L^{-2}.T^{-1}]}{[M.L^{-1}.T^{-1}]}$$
$$Pr=\frac{C_p\,\mu}{k_L}=\frac{[L^2.T^{-2}.K^{-1}]\,[M.L^{-1}.T^{-1}]}{[M.L^{1}.T^{-3}.K^{-1}]} \quad (26)$$

where, G is the coolant mass flow rate for each coolant area and μ is the coolant viscosity

2.5. Modeling assumptions and implementation in the MTRDYN

Since a heat transfer was considered on the thermal module of MTRDYN, single-phase fluid was facilitated in the axial direction only (Z-axis), with the inlet coolant in the top side of the fuel element was considered, the forced coolant flow being modeled was in line with the gravity. The energy balance from the radial (x-axis) heat transfer was solved for each mesh of the fission region. On the other hand, the thermal properties of material, such as the fuel meat thermal capacity, density, and thermal conductivity, are considered as constant in MTRDYN, including the cladding thermal properties and the solid material dimension (fuel thickness, cladding thickness, and coolant width). The water properties being used in MTRDYN came from the steam table data provided by JAERI, but MTRDYN terminates the simulation when the coolant temperature has been exceeding the coolant temperature limit of 374.15 K (101 °C), which surpasses the boiling temperature of water at atmospheric pressure. By this approach, any dynamic calculation, starting from a steady state with feedback or transient calculation, will be terminated once the coolant temperature exceeds, to make sure that the coolant is still in the liquid phase and the correlation being used on the single-phase fluid dynamics is implemented properly.

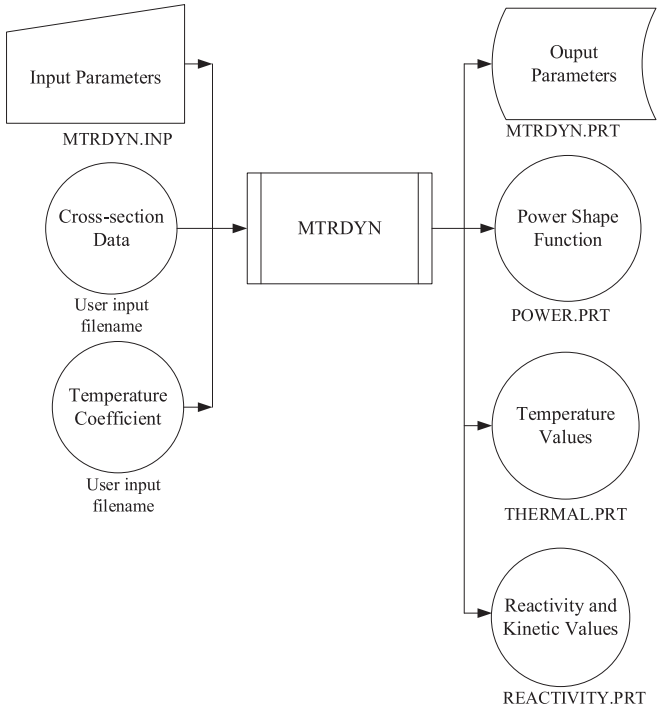

Fig. 1. MTRDYN input/output file structure (Pinem et al., 2022).

The input and output files structure of the MTRDYN code is shown in Fig. 1. Neutronic parameters such as power density are used as inputs in the thermohydraulic simulation to determine the fuel element temperature distribution. The coupling between neutronic and thermohydraulic results was done iteratively since the temperature distribution affects neutronic parameters through the few-group cross-section used in the diffusion solver. Iterations are carried out until the convergence criterion is obtained, and the calculated power and temperature distribution are reported for specific operating conditions of the reactor.

By this approach, the convergence criteria being considered mostly came from the diffusion iteration, with typical flux and eigenvalue convergence criteria (inner and outer). The convergence check for neutronic and thermal-hydraulic was limited to the number of iterations being used by the user, while during MTRDYN steady state calculation, the considered convergence criteria was the total group neutron flux relative difference. By this approach, the user could control the time step being used for solving the kinetic equation and consider using a proper number of neutronic and thermal-hydraulic iterations. A small-time step could give a benefit in the of stability, but the repeated diffusion iteration for each new group constant based on the new temperature distribution was a challenge in a sequential calculation implemented in MTRDYN. The output of the MTRDYN code includes neutronic, kinetic, and thermal-hydraulic parameters, reported based on the time step being applied. In a steady state calculation, even when the transient input was used to calculate the dynamic response, the calculated result could be seen as an almost constant parameter reported since there is no change in the core reactivity, flow rate, and coolant properties, with minor reactivity feedback in a steady state calculation model using the dynamic feature of the MTRDYN.

Table 1
Main design data of RSG-GAS (Jujuratisbela et al., 1995).

Parameters	unit	First core	Sixth core
Nominal power	MWth	10.6	30.0
Number of FEs		12	40
Number of CEs		6	8
Number of beryllium blocks		42	30
Primary coolant flow	m^3/h	2550	3300
Average flow rate of fuel element	m^3/h	51.78	47.01
Fuel & control element dimension	mm	77.1× 81× 600	
Thickness of fuel plate	mm	1.3	
Coolant channel thickness	mm	2.55	
Number of plates per fuel element		21	
Number of plates per control element		15	
Cladding material of fuel plate		AlMg2	
Cladding thickness of fuel plate	mm	0.38	
Fuel plate dimensions	mm	0.54 × 62.75 × 600	
Fuel meat material		U_3O_8-Al	
U-235 enrichment	w/o	19.75	
Uranium density in fuel meat	g/cc	2.96	

3. RSG-GAS reactor core

The Typical Working Core (TWC) configuration of the RSG-GAS reactor was achieved following six core transitions, with the addition of fuel and reflectors (Jujuratisbela et al., 1995; PRSG, 1988). The first core consisted of 12 fuel elements (FE) and 6 control elements (CE) to facilitate control rods insertion, while operating at a maximum power of 10.6 MW. The TWC core consists of 40 FE and 8 control elements (CE), with a maximum power of 30 MW. The main core data of the RSG-GAS reactor are presented in Table 1.

The core was arranged in a 10 × 10 grid with a spacing of 81 × 77 mm. The fuel elements use low-enriched uranium (LEU) of the MTR-type, consisting of 21 parallel fuel plates with a thickness of 0.54 mm for the fuel and 0.38 mm for each cladding side. The total fissionable mass of U-235 in a single fuel element was 250 g (PRSG, 1988). For reactor control and shutdown, fork-type absorbers containing Ag-In-Cd are used by replacing six outer fuel plates from a standard fuel element. As a result, the control element has a nominal U-235 loading of 178.57 g. Fig. 2 illustrates the fuel and control elements. To enhance reactor economic efficiency, the core was surrounded by beryllium reflector elements, with beryllium reflector blocks positioned in an L-shape around the active core, while Fig. 3 shows the TWC core configuration.

The coolant channel (gap) between the fuel plates has a thickness of 2.55 mm, with demineralized light water serving as the coolant and moderator in the reactor core. Heat was extracted via the reactor coolant system that operates in both primary and secondary loops. In the primary loop (reactor pool), water flows downward between the fuel plates with a minimum flow rate of 800 kg/s at 30 MW operation (Isnaini et al., 2020), making the average coolant velocity in each channel was 3.8 m/s (Subekti et al., 2013).

4. Methodologies

4.1. Measurement of excess reactivity

The first criticality with specific fuel loading of the reactor core provides the reference point for calculating excess reactivity, including adding fuel elements and reflector elements for excess reactivity. In the first core, the first criticality was obtained with nine fresh fuel elements, while the control rod bank was positioned at 600 mm and the regulating rod at 475 mm. To achieve the desired excess reactivity, additional FEs were loaded to the core. The reactivity was determined by calibrating the regulating rod after each fuel loading, with the reactivity measurements were conducted through the compensation method utilizing a reactivity meter. Hence, the excess reactivity of the RSG-GAS first core was achieved with 12 FEs, 6 CRs, and 42 beryllium blocks, while in the sixth core, excess reactivity was achieved with 40 FEs, 8 CRs, and 30 reflector elements. The experiment on the core reactivity and kinetic parameter was conducted at a low power condition, with the reactivity experiment mostly conducted on the near critical source-free condition, making the condition analogous to the cold zero power (CZP) without Xe and Sm in the core.

4.2. Measurement of coolant and cladding temperature of fuel element

Fission heat generated in the fuel meat was conducted to the coolant through the cladding material. However, thermal resistance in the fuel, cladding, and coolant leads to a temperature gradient, which induces a specific heat flux. Therefore, the reactor coolant flow and the generated fission heat are controlled to prevent coolant and fuel cladding temperatures from exceeding their limit values and maintain an adequate safety margin. The coolant and cladding temperature measurements were conducted during the commissioning of the RSG-GAS reactor to

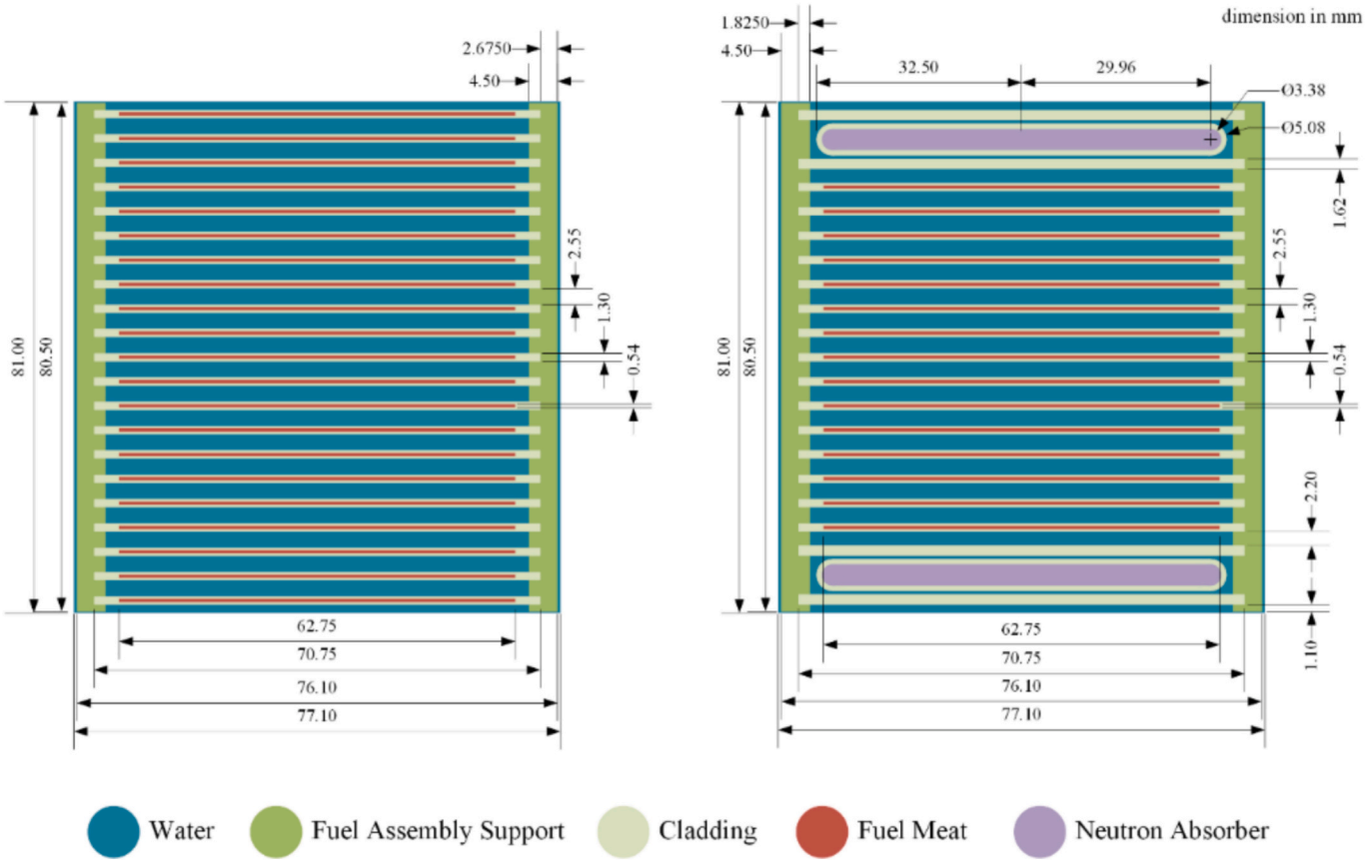

Fig. 2. Standard fuel element (left) and control element (right) (Pinem et al., 2022; Pinem et al., 2025c; Pinem et al., 2025a).

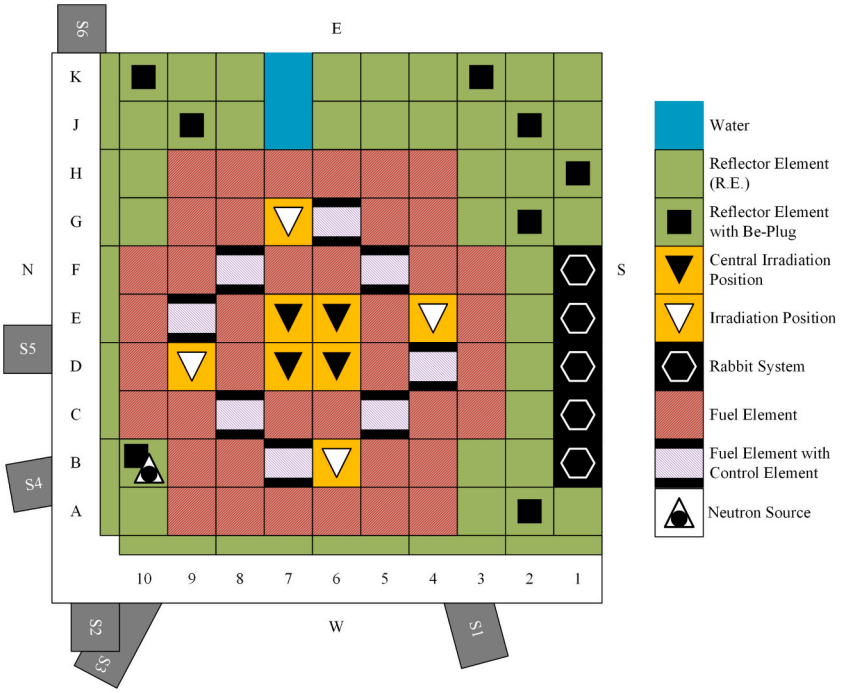

Fig. 3. The RSG-GAS TWC configuration.

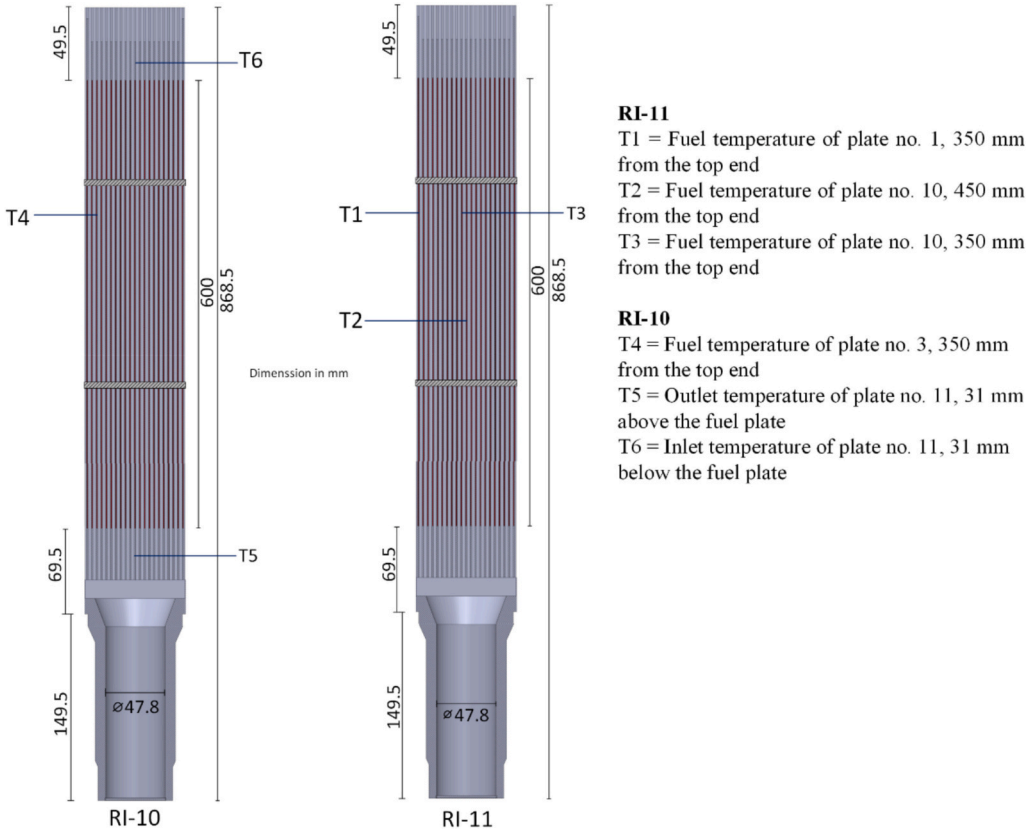

Fig. 4. Thermocouples' positions in the Instrumental Fuel Element.

Table 2
Reactor operating conditions of the first and sixth cores.

Parameters	First core		Sixth core
Reactor power (MW)	7	9	25
Coolant flow rate (m^3/h)	2550	2550	3300
Position bank (mm)	373	373	260
Position regulating rod (mm)	373	373	258
Position RI-10 in core	D-7	D-7	E-8
Position RI-11 in core	E-6	E-6	D-5

verify the fuel cladding temperatures and the surrounding coolant. The measurements utilized two instrumented fuel elements - IFEs, RI-10 and RI-11. In these terms, fuel-cladding temperatures were used since both IFE, RI-10, and RI-11 were equipped with thermocouples directly welded to the cladding surface on the fuel plate, which are shown in Fig. 4.

RI-10 had three thermocouples, T4, T5, and T6, with T6 on top could be used to measure the inlet coolant temperatures, T5 at the bottom was used to measure the outlet temperature, and T4, placed 350 mm from the top of the fuel plate 3, to measure its fuel-cladding temperature. RI-11 was equipped with three thermocouples to measure the fuel-cladding temperature at fuel plate no. 1 (T1) and fuel plate no. 10 (T3) at 350 mm from the top, while T2 is for fuel plate no 10 at 450 mm from the top. A six-channel recorder was used at that time to record the thermocouple signals from the instrumented fuel elements. The measurements were carried out by increasing the reactor power to the desired level and maintaining it (constant power) for 48 h without changing the control rod positions. The operating conditions during the experiment are presented in Table 2.

4.3. MTRDYN model for calculations

The MTRDYN program requires a complete set of macroscopic cross-section data, including absorption, fission, diffusion, and scattering, as well as reactivity coefficients for fuel and moderator temperature. The fuel and control elements' cross-section data were obtained through the reflective assembly level model. In addition to the fuel and control elements, the RSG-GAS reactor core includes several non-fuel components, such as dummy elements, reflector blocks, rabbit system facilities, and others. Therefore, a full core model was utilized to generate few-group constants for non-fuel components. A continuous-energy Monte Carlo code, Serpent 2 (Leppänen et al., 2015), was used to generate the cross-section data for the fuel and control elements of the RSG-GAS reactor. The few-group cross-section was generated with the continuous energy nuclear data library of ENDF/B-VIII.0 (Brown et al., 2018), which collapsed into a four-group (4G) energy structure with energy bounds of 1.00E+01, 8.21E-01, 5.54E-03, 6.25E-07, and 1.00E-11 MeV.

The RSG-GAS core developed for MTRDYN consists of a simple Cartesian model of the core, as shown in Fig. 3, and an additional coolant region in both radial and axial directions, with a height of up to 60 cm on top to facilitate the positioning of the control rod during a steady-state experiment with IFE in the core. The fuel and reflector region was modeled based on the core grid size (7.71 × 8.1 cm) following the control rod blades position, with a node size of 2.5 cm for the non-fuel region, while the fuel region used a finer mesh of 1.5–2.0 cm in radial and axial direction. The axial fuel region consists of not less than 2 regions to accommodate the control rod insertion, such as ~20 radial reparation for control rod position in core and the remaining absorber region on top of the core, while the reflector block was modeled as 6 separated layers of beryllium block to mimic the separation being used on the Serpent model. The MTRDYN steady state calculation being considered was utilizing an inlet coolant temperature of 36 °C at 2 bar for two selected cores, the first core (7 and 9 MW) and the sixth core (25 MW), to facilitate the aforementioned core condition shown in Table 2.

Table 3
Kinetic parameters of the first and sixth core.

Parameters	1st Core		6th core	
	Experiment	MTRDYN	Experiment	MTRDYN
Excess reactivity (%)	8.46 ± 0.02	8.30 (−1.90 %)[a]	9.87 ± 0.01	9.89 (0.21 %)
Control rod worth (%)	−17.79 ± 0.04	−18.17 (−2.17 %)	−15.52 ± 0.04	−14.91 (3.93 %)

[a] (MTRDYN/Experiment- 1) × 100 %.

5. Result and discussion

5.1. Excess reactivity

Excess reactivity is considered a key factor in maintaining the safety and reliability of nuclear reactor operations, as it refers to the additional reactivity margin for the reactor core to operate during its core cycle length. The amount of fissile material in the core continuously decreases during reactor operation. Additionally, changes in reactivity occur due to fuel depletion, fission product poisons, and the loss of reactivity caused by temperature changes in the fuel, moderator, and structural materials, among others. To sustain operation throughout a fuel cycle, the reactor must maintain sufficient excess reactivity to offset reactivity losses occurring during the cycle. Excess reactivity was derived by calculating the effective multiplication factor (keff) in the calculation, but from the perspective of excess reactivity experiment, it came from the reactivity measured during the fuel element loaded to the core. Table 3 presents the calculated excess reactivity and control rod worth for the first and sixth cores in cold zero power (CZP). The difference in excess reactivity between the experiment and the calculations for the first core is −1.33 % (−160.0 pcm), and 0.21 % (20.0 pcm) for the sixth core. A discrepancy of 2.17 % and − 3.90 % was observed between the experimental and calculated total control rod worth for the first and sixth cores, respectively. The control rod worth by MTRDYN was calculated by the up-down method, which is subtracting the reactivity of the core with all control rods out (ARO) from the core with all control rods in (ARI). On the other hand, the experiment came from the sum up of each control rod being measured with the compensation method, in a critical CZP condition. Overall, the MTRDYN code provides reasonable

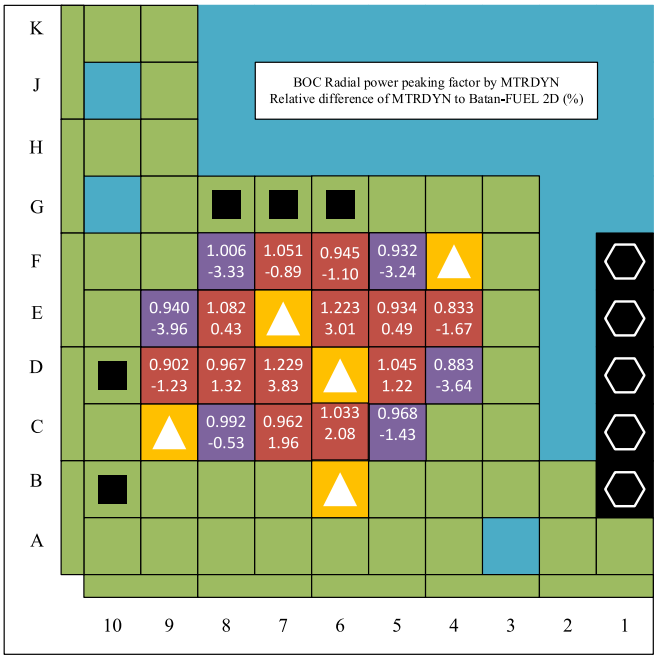

Fig. 5. Distribution of first core radial power fraction.

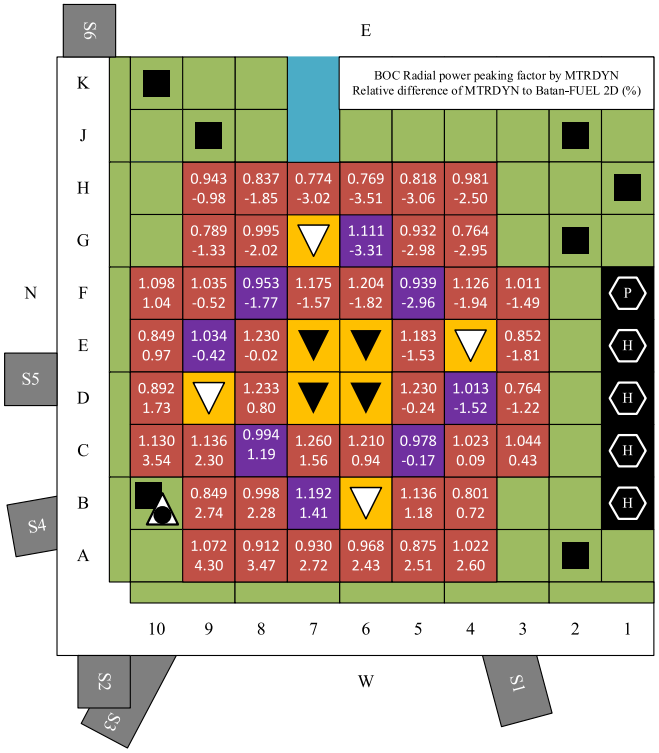

Fig. 6. Distribution of sixth core radial power fraction.

results of excess reactivity and total control rod worth compared to experimental data.

5.2. Power peaking factor radial and axial

The power peaking factor (PPF), defined as the maximum local power density divided by the core's average power density, is essential for maintaining the safe and efficient operation of nuclear reactors. PPF is crucial to ensure that the reactor operates within safe temperature limits to prevent fuel meltdown. The results of the radial PPF calculations for the first core and the sixth core are shown in Figs. 5 and 6. The radial PPF values are compared against the results obtained from the Batan-FUEL code, which has been verified with Serpent 2 for radial PPF

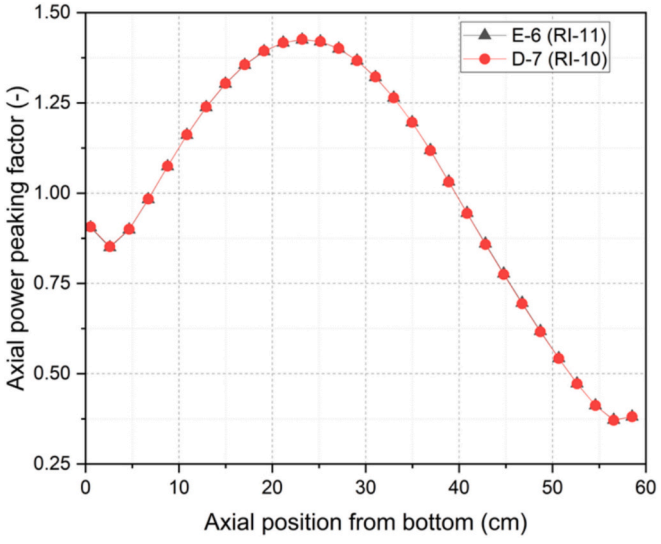

Fig. 7. Axial power distribution of the 1st core for RI-10 and RI-11.

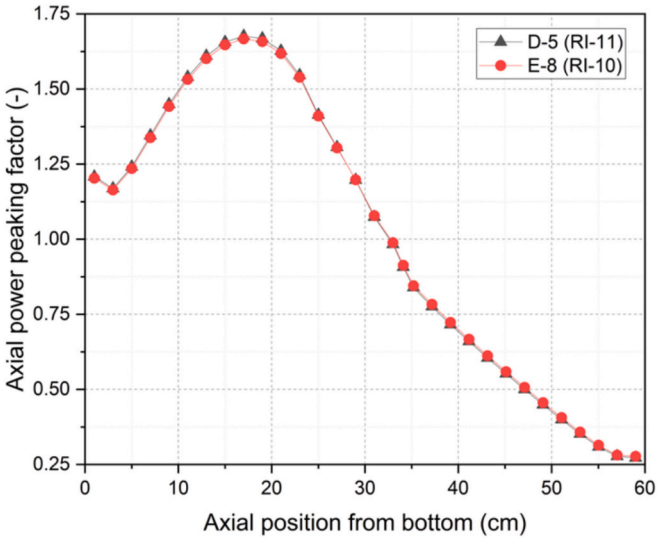

Fig. 8. Axial power distribution of the 6th core for RI-10 and RI-11.

calculations (Pinem et al., 2023). The PPF calculations using the MTRDYN code show a maximum difference of 3.96 % for the first core and 4.3 % for the sixth core.

Axial PPF is an important metric in neutronic parameter calculations because it is related to power distribution along the reactor core. This parameter is a crucial component in the power distribution to ensure that the reactor operates within safe temperature limits. The fuel cladding temperature reported in this study was the hottest temperature at positions D-7 (RI-10) and E-7 (RI-11) for the first core, and E-8 (RI-10) and E-5 (RI-11) for the sixth core.

Since the fuel cladding temperature depends on the axial power distribution for the fuel elements, the fuel elements located at specific positions could have the maximum axial power fraction, which depends on various parameters, such as the control rod position and the fuel burnup distribution. The selection of IFE positions (RI-10 and RI-11) was considered for a similar reason of measuring the fuel cladding temperature in the hottest region in the core. The axial PPF was calculated at the aforementioned IFE positions during the measurement of fuel cladding temperature, with the calculation results for the first and sixth cores shown in Figs. 7 and 8. The maximum axial PPF for the first and sixth cores are 1.42 and 1.67, respectively. Based on the safety analysis reactor (SAR), the maximum allowed axial PPF is 1.79 (RSG-Batan, 2011).

5.3. Kinetic parameters

As seen in Table 4, kinetic parameters calculated using MTRDYN were compared with the kinetic data reported on the RSG-GAS Safety Analysis Report (SAR). The kinetic data on SAR were prepared by Interatom for the RSG-GAS 1st and 6th cores, which were calculated using their code, such as IAFUEL developed with ENDF/B-V.0. The calculation was carried out at the beginning of each core (BOC) with its corresponding power, with the kinetic parameters shown a good

Table 4
Comparison of kinetic parameters for oxide and SAR.

Reactor parameters	First core		Sixth core	
	SAR	MTRDYN	SAR	MTRDYN
Total delayed neutron fraction. β_{eff} (pcm)	765.00	728.00 (−4.84 %)[a]	719.00	711.10 (−1.10 %)
Prompt neutron lifetime ℓ (μs)	61.30	59.47 (−2.99 %)	64.51	61.82 (−4.17 %)

[a] (MTRDYN/SAR- 1) × 100 %.

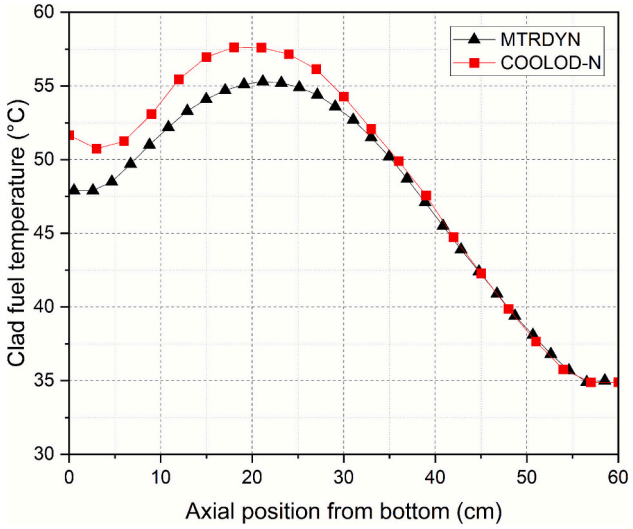

Fig. 9. The average cladding temperature for RI-11 at the first core, 7 MW.

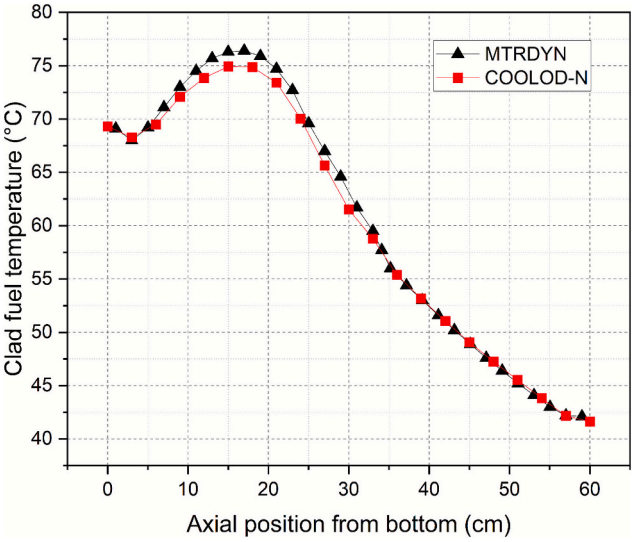

Fig. 10. The average cladding temperature for RI-11 at the sixth core, 25 MW.

agreement to the experiment on kinetic parameter that been carried out using the rod drop method (Sembiring and Pinem, 2002). The calculated effective delayed neutron fraction (βeff) for the first core and the sixth core shows differences of 4.84 % and 1.10 %, respectively, compared to the SAR. The calculated prompt neutron lifetime shows the differences of 2.99 % for the first core and 4.64 % for the sixth core.

5.4. Steady state thermal-hydraulic

Thermal-hydraulic studies are crucial in the safety analysis of nuclear reactor operations. Accurate calculations are needed to predict the reactor's operating conditions and ensure the safe operation of nuclear reactors. The average axial cladding temperature distribution calculation at position E-6 for the first core at 7 MW is shown in Fig. 9, while Fig. 10 shows the cladding temperature at position D-5 for the sixth core at 25 MW. The calculations with MTRDYN are compared with the COOLOD-N program. The COOLOD-N program was routinely used at the RSG-GAS reactor to determine the fuel temperature (Hastuti et al., 2000; Hastuti and Subekti, 2013). The COOLOD-N model of the IFE fuel position uses the axial power distribution shown in Figs. 7 and 8 with the average power density provided by MTRDYN, which differs from the full

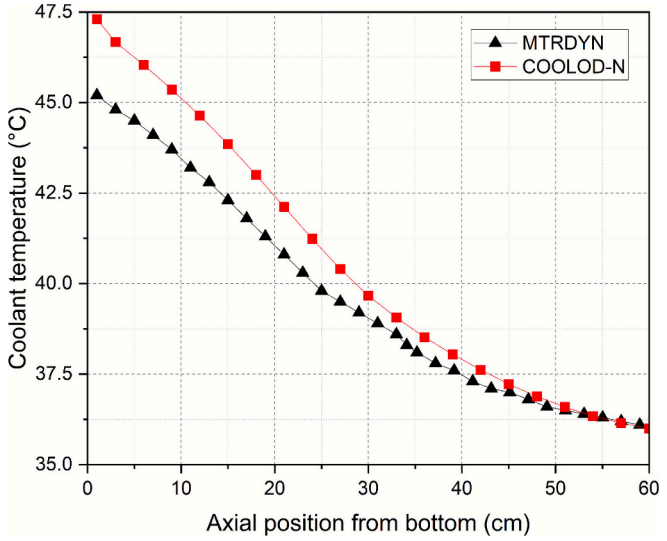

Fig. 11. The average cladding temperature for RI-11 at the sixth core, 25 MW.

Table 5
Measured data and MTRDYN results for RSG-GAS First Core at 7 MW power.

Reactor parameters	Measured data	MTRDYN	Difference (°C)
Temperature T1 (°C)	63.36 ± 0.38	59.70	−3.66 (−5.78 %)[a]
Temperature T2 (°C)	47.40 ± 0.51	49.00	1.60 (3.38 %)
Temperature T3 (°C)	47.40 ± 0.25	48.40	1.00 (2.10 %)
Temperature T4 (°C)	54.30 ± 0.25	55.90	1.60 (2.95 %)
Temperature T5 (°C) bottom clad. (*outlet*)	35.28 ± 0.25	33.80	−1.48 (−4.20 %)
Temperature T6 (°C) top clad. (*inlet*)	28.58 ± 0.25	28.50	−0.08 (−0.28 %)

[a] (MTRDYN/Experiment-1) × 100 %.

Table 6
Measured data and MTRDYN results for RSG-GAS First Core at 9 MW power.

Reactor parameters	Measured data	MTRDYN	Difference (°C)
Temperature T4 (°C)	61.83 ± 0.25	59.60	−2.23 (−3.61 %)[a]
Temperature T5 (°C) bottom clad. (*outlet*)	38.15 ± 0.25	37.10	−1.05 (−2.75 %)
Temperature T6 (°C) top clad. (*inlet*)	30.05 ± 0.25	30.10	0.05 (0.17 %)

[a] (MTRDYN/Experiment-1) × 100 %.

core 3D model being implemented in MTRDYN. The relative difference was described as (MTRDYN/COOLOD-N- 1) × 100 %

The maximum cladding temperature for the first core calculated by the MTRDYN code was 55.3 °C, which is lower than COOLOD-N with a relative difference of −4.19 % compared to COOLOD-N. For the sixth core, the maximum temperature calculated was 76.4 °C, with a 1.92 % difference compared to COOLOD-N. Meanwhile, the calculated coolant temperature for the sixth core is shown in Fig. 11. When compared to COOLOD-N, the maximum relative difference was −4.64 %, with the discrepancies coming from the coolant temperature being used by COOLOD-N compared to the JAERI steam table being compiled for the MTRDYN. The results for both cladding and coolant temperatures show no significant difference between the calculations using MTRDYN and COOLOD-N, with the difference less than 4 °C.

The analysis of nuclear fuel cladding temperature behavior is one of the most important aspects of nuclear safety. If the temperature of the

Table 7
Measured data and MTRDYN results for Sixth Core at 25 MW power.

Reactor parameters	Measured data	MTRDYN	Difference (°C)
Temperature T1 (°C)	84.30 ± 0.38	83.50	−0.80 (−0.95 %)[a]
Temperature T2 (°C)	69.20 ± 0.51	70.90	1.70 (2.46 %)
Temperature T3 (°C)	64.90 ± 0.25	63.80	−1.10 (−1.69 %)
Temperature T4 (°C)	75.10 ± 0.25	71.20	−3.90 (−5.19 %)
Temperature T5 (°C) bottom clad. (*outlet*)	42.50 ± 0.25	43.62	1.12 (2.64 %)
Temperature T6 (°C) top clad. (*inlet*)	36.00 ± 0.25	36.00	0.00 (0.00 %)

[a] (MTRDYN/Experiment-1) × 100 %.

fuel element increases beyond critical values, the fuel element melts down, causing fuel damage. Therefore, the analysis and calculation of fuel element meltdown in nuclear reactors is a crucial issue to be addressed for reactor operation safety. A comparison was made between the thermal-hydraulic outputs of the MTRDYN code and the experimental results for the RSG-GAS first core configuration. For the first core, the calculation results at 7 MW and 9 MW power are shown in Tables 5 and 6. At 9 MW power, only RI-10 was used in the measurements. The maximum discrepancies are 3.66 °C (5.78 %) between the calculation and experimental results at 7 MW, and it lowers to 2.23 °C (3.61 %) at 9 MW conditions.

For the sixth core, the calculation results at 25 MW power are shown in Table 7 with the maximum difference between the calculated results and the experimental data was 3.90 °C (5.19 %). With the discrepancies not exceeding 4 °C, the calculated temperature from the MTRDYN is in good agreement with the experiment, presenting its capabilities for determining the coolant and fuel cladding temperatures of the RSG-GAS as a kind of MTR-type research reactor.

6. Conclusion

The coupled neutronic and thermal-hydraulic code, MTRDYN, has been developed for plate-type fuel reactors. To validate this code, neutronic and thermal-hydraulic parameters were calculated and compared with experimental results during the RSG-GAS commissioning. The calculated excess reactivity was in good agreement with a maximum deviation of 1.33 % from experiments. The calculated fuel-cladding temperatures showed a maximum difference of 5.78 % compared to measurements, which mostly below 4 °C. In the other hand, calculated radial PPF showed a maximum deviation of 4.3 % compared to the Batan-FUEL calculations. Based on these results, the MTRDYN demonstrates good consistency in determining the RSG-GAS neutronic and thermal-hydraulic parameters.

CRediT authorship contribution statement

Surian Pinem: Writing – review & editing, Writing – original draft, Validation, Software, Investigation, Formal analysis, Data curation, Conceptualization. **Farisy Yogatama Sulistyo:** Writing – review & editing, Writing – original draft, Visualization, Formal analysis, Data curation. **Peng Hong Liem:** Writing – review & editing, Writing – original draft, Validation, Software. **Sukmanto Dibyo:** Writing – review & editing, Software, Investigation, Formal analysis. **Wahid Luthfi:** Writing – review & editing, Writing – original draft, Visualization.

Funding details

This research received no external funding.

Declaration of competing interest

The authors declare that they have no known competing financial interests or personal relationships that could have appeared to influence the work reported in this paper.

Acknowledgment

Thank you to the head of the Research Center for Nuclear Reactor Technology (PRTRN) of the Research Organization for Nuclear Energy, the National Research and Innovation Agency (ORTN-BRIN), for supporting this research.

Data availability

All relevant data for this study have been described in this manuscript.

References

Akbas, S., Martinez-Quiroga, V., Aydogan, F., Ougouag, A.M., Allison, C., 2015. Survey of coupling schemes in traditional coupled neutronics and thermal-hydraulics codes. In: ASME International Mechanical Engineering Congress and Exposition, Proceedings (IMECE), 6B-2015, IMECE2015-52990. https://doi.org/10.1115/IMECE201552990.

Akbas, S., Quiroga, V.M., Aydogan, F., Allison, C., Ougouag, A.M., 2019. Thermal-hydraulics and neutronic code coupling for RELAP/SCDAPSIM/MOD4.0. Nucl Eng Des 344 (January), 174–182. https://doi.org/10.1016/j.nucengdes.2019.01.009.

Alnaqbi, J., Hartanto, D., Alnuaimi, R., Imron, M., Gillette, V., 2022. Static and transient analyses of advanced power reactor 1400 (APR1400) initial core using open-source nodal core simulator KOMODO. Nucl Eng Technol 54 (2), 764–769. https://doi.org/10.1016/j.net.2021.08.012.

Boustani, E., Khakshournia, S., 2020. An investigation for the fuel temperature of the Tehran research reactor during a complete loss of coolant accident. Prog Nucl Energy 129 (October 2018), 103489. https://doi.org/10.1016/j.pnucene.2020.103489.

Brown, D.A., Chadwick, M.B., Capote, R., Kahler, A.C., Trkov, A., Herman, M.W., Sonzogni, A.A., Danon, Y., Carlson, A.D., Dunn, M., Smith, D.L., Hale, G.M., Arbanas, G., Arcilla, R., Bates, C.R., Beck, B., Becker, B., Brown, F., Casperson, R.J., Zhu, Y., 2018. ENDF/B-VIII.0: the 8th major release of the nuclear reaction data library with CIELO-project cross sections, new standards and thermal scattering data. Nuclear Data Sheets 148, 1–142. https://doi.org/10.1016/j.nds.2018.02.001.

Cardoni, J.N., Rizwan-uddin, 2011. Nuclear reactor multi-physics simulations with coupled MCNP5 and STAR-CCM+. In: International Conference on Mathematics and Computational Methods Applied to Nuclear Science and Engineering (M&C 2011), pp. 1–15.

Castellanos-Gonzalez, D.A., Moreira, J.M.L., Maiorino, J.R., Carajilescov, P., 2018. Validation of the COTENP code: a steady-state thermal-hydraulic analysis code for nuclear reactors with plate type fuel assemblies. Sci Technol Nucl Install 2018. https://doi.org/10.1155/2018/9874196.

Dibyo, S., Pinem, S., Widodo, S., 2021. Transient calculation on TRIGA 2000 of plate-type fuel element using RELAP5, EUREKA2/ R, and MTRDYN codes. Nucl Technol Radiat Protect 36 (3), 211–218. https://doiserbia.nb.rs/img/doi/1451-3994/2021/1451-39942103211D.pdf.

Dibyo, S., Pinem, S., Sulistyo, F.Y., Sriwardhani, V.I., 2024. CFD simulation on sub-channel blockage in the fuel plate of RSG-GAS reactor. Prog Nucl Energy 170 (September 2023), 105155. https://doi.org/10.1016/j.pnucene.2024.105155.

Duderstadt, J.J., Hamilton, L.J., 1977. Nuclear Reactor Analysis. John Wiley & Sons, Inc.

Hastuti, E.P., Subekti, M., 2013. Thermalhydraulic analysis of U-7Mo/Al and U-6ZR/Al experimental fuel element in RSG-GAS BY using COOLOD-N2, NATCON and CFD-3D. Urania Jurnal Ilmiah Daur Bahan Bakar Nuklir 19 (1), 1–14.

Hastuti, E.P., Isnaini, M.D., Sufmawan, A., 2000. Analisis Pengujian Elemen Bakar Dummy Uji Silisida Aspek Keselamatan RSG-GAS. In: Prosiding Presentasi Ilmiah Daur Bahan Bakar Nuklir V, P2TBDU & P.

Hu, J., Rizwan-uddin., 2008. Coupled neutronics and thermal-hydraulics simulations using MCNP and FLUENT. Adv Muti Phys React Sim. 606. https://verl.npre.illinois.edu/Documents/C-08-01.pdf.

Iliuk, I., Balthazar, J.M., Tusset, Â.M., Piqueira, J.R.C., 2016. Thermal-hydraulic analysis under partial loss of flow accident hypothesis of a plate-type fuel surrounded by two water channels using RELAP5 code. Adv Mech Eng 8 (1), 1–8. https://doi.org/10.1177/1687814015626369.

Imron, M., 2019. Development and verification of open reactor simulator ADPRES. Ann Nucl Energy 133, 580–588. https://doi.org/10.1016/j.anucene.2019.06.049.

Imron, M., Hartanto, D., 2021. Pressurized water reactor mixed oxide/UO2 transient benchmark calculations using Monte Carlo serpent 2 code and open nodal core simulator ADPRES. J Nucl Eng Radiat Sci 7 (3), 1–8. https://doi.org/10.1115/1.4048764.

INL, I.N.L., 2025. MOOSE-Based/Wrapped Multiphysics Nuclear Reactor Simulations. Moose Documentation Retrieved September 26, 2025, from https://mooseframework.inl.gov/virtualtestbed/vtb_tutorials/multiapps/chp_3_applications.html.

Isnaini, M.D., Kuntoro, I., Muh. Subekti., 2020. Transient analysis of simultaneous LOFA and RIA in RSG-GAS reactor after 32 years operation. Jurnal Teknologi Reaktor Nuklir Tri Dasa Mega 22 (3), 111–119. https://doi.org/10.17146/tdm.2020.22.3.5944.

Jo, D., Park, J., Chae, H., 2014. Development of thermal hydraulic and margin analysis code for steady state forced and natural convective cooling of plate type fuel research reactors. Prog Nucl Energy 71, 39–51. https://doi.org/10.1016/j.pnucene.2013.11.006.

Jujuratisbela, U., Arbie, B., Pinem, S., Tukiran, Suparlina, L., & Singh, O. P., 1995. Kinetics parameter measurements on RSG-GAS, a low enriched fuel reactor. In: International Conference on Research Reactors: Safe Management and Effective Utilization, pp. 333–350.

Kaminaga, M., 1994. COOLOD-N2 a Computer Code, for the Analyses of Steady-State Thermalhydraulics in Research Reactors (p. JAERI-M-94-052). Japan Atomic Energy Research Institute.

Kuntoro, I., Pinem, S., Sembiring, T.M., Haryanto, D., Purwanto, S., 2021. Evaluation of equilibrium Core operation of the Rsg-gas reactor. Jurnal Teknologi Reaktor Nuklir Tri Dasa Mega 23 (1), 15. https://doi.org/10.17146/tdm.2021.23.1.6150.

Lago, E., Dominguez, D.S., Mazaíra, L.R., 2024. Multiphysics computational Modeling of nuclear reactors small size through the coupling of serpent codes and Fluent. Braz J Radiat Sci 12 (3), e2425. https://doi.org/10.15392/2319-0612.2024.2425.

Leppänen, J., 2022. Methodology, applications and performance of the CAD-based geometry type in the serpent 2 Monte Carlo code. Ann Nucl Energy 176. https://doi.org/10.1016/j.anucene.2022.109259.

Leppänen, J., Pusa, M., Viitanen, T., Valtavirta, V., Kaltiaisenaho, T., 2015. The serpent Monte Carlo code: status, development and applications in 2013. Ann Nucl Energy 82, 142–150.

Liem, P.H., 1994. Development and verification of Batan's standard, two-dimensional multigroup neutron diffusion code. Atom Indonesia 20 (1), 1–19.

Liem, P.H., 1996. Batan-fuel: a general in-Core fuel management code. Atom Indonesia 22 (2), 67–80.

Liem, P.H., 1999. Validation of BATAN'S standard 3-D diffusion code, BATAN-3DIFF, on the first Core of RSG GAS. Atom Indonesia 25 (1), 47–53.

Liem, P.H., Sembiring, T.M., 2010. Design of transition cores of RSG GAS (MPR-30) with higher loading silicide fuel. Nucl Eng Des 240 (6), 1433–1442. https://doi.org/10.1016/j.nucengdes.2010.01.028.

Liem, P.H., Pinem, S., Sembiring, T.M., Tran, H., 2016. Status on development and verification of reactivity initiated accident analysis code for PWR (NODAL3). Nucl Sci Tech 6 (1), 1–13.

Loi, L., Riva, S., Introini, C., Giacobbo, F., Wang, X., Cammi, A., 2024. OFELIA: an OpenMC-FEniCSx coupling for neutronic calculation with temperature feedback. Nucl Eng Des 428 (July), 113480. https://doi.org/10.1016/j.nucengdes.2024.113480.

Novak, A.J., Andrs, D., Shriwise, P., Fang, J., Yuan, H., Shaver, D., Merzari, E., Romano, P.K., Martineau, R.C., 2022. Coupled Monte Carlo and thermal-fluid modeling of high temperature gas reactors using cardinal. Ann Nucl Energy 177, 109310. https://doi.org/10.1016/j.anucene.2022.109310.

Operasi Reaktor, B., 1987. Laporan Operasi Reaktor GA Siwabessy.

Osusky, F., Cerba, S., Luley, J., Vrban, B., Hascik, J., 2018. Coupled simulation of gas cooled fast reactor fuel assembly with Nestle code system. Acta Polytech CTU Proc 14 (1), 34. https://doi.org/10.14311/app.2018.14.0034.

Passons, B., Tsvetkov, P., 2022. Design and performance analysis of a mobile, land-based micro-reactor. Ann Nucl Energy 165, 108688. https://doi.org/10.1016/j.anucene.2021.108688.

Pater, M., 2019. Multiphysics Simulations of Molten Salt Reactors Using the Moltres Code. September.

Pinem, S., Sembiring, T.M., 2006. Application of neutronics modelling on the transient simulation of RSG-GAS reactor. In: Proc. of the International Conference on Mathematics and Natural Science, Bandung, Indonesia, pp. 1056–1059.

Pinem, S., Sembiring, T.M., 2019. Accuracy of Batan-3DIFF and MCNP6 codes for thermal neutron flux distribution at the irradiation position of RSG-GAS reactor. Int J Nucl Energy Scie Technol 13 (4), 295–312. https://doi.org/10.1504/IJNEST.2019.106050.

Pinem, S., Liem, P.H., Sembiring, T.M., Surbakti, T., 2016a. Fuel element burnup measurements for the equilibrium LEU silicide RSG GAS (MPR-30) core under a new fuel management strategy. Ann Nucl Energy 98. https://doi.org/10.1016/j.anucene.2016.08.010.

Pinem, S., Sembiring, T.M., Liem, P.H., 2016b. NODAL3 sensitivity analysis for NEACRP 3D LWR Core transient benchmark (PWR). Sci Technol Nucl Install 2016, 1–11. https://doi.org/10.1155/2016/7538681.

Pinem, S., Sembiring, T.M., Surbakti, T., 2020a. Reactivity insertion accident analysis during uranium foil target irradiation in the RSG-GAS reactor Core. Nucl Technol Radiat Protect 35 (3), 1–7.

Pinem, S., Surbakti, T., Liem, P.H., 2020b. Safety analysis of the TRIGA 2000 U3Si2-Al fuel Core under reactivity insertion accidents. At Indones 46 (1), 33–39.

Pinem, S., Dibyo, S., Luthfi, W., Wardhani, V.I.S., Hartanto, D., 2022. An improved steady-state and transient analysis of the RSG-GAS reactor Core under RIA conditions using MTR-DYN and EUREKA-2/RR codes. Sci Technol Nucl Install 2022. https://doi.org/10.1155/2022/6030504.

Pinem, S., Hartanto, D., Liem, P.H., Luthfi, W., 2023. Improvement of few-group homogenized cross-sections for RSG-GAS in-Core FUEL management code Batan-FUEL. J Nucl Eng Radiat Sci 9 (3), 1–7. https://doi.org/10.1115/1.4056603.

Pinem, S., Luthfi, W., Liem, P.H., 2024. Verification of NODAL3 code with PWR MOX/UO2 core transient benchmark. Nucl Eng Des 424 (February), 113326. https://doi.org/10.1016/j.nucengdes.2024.113326.

Pinem, S., Isnaini, M.D., Luthfi, W., 2025a. Comparison of Neutronic and Thermal-Hydraulic Performance of KOMODO, NODAL3, and COBRA for Steady-State Operation of APR1400. Gazi Univ J Sci 38 (3), 1431–1447. https://doi.org/10.35378/gujs.1508000.

Pinem, S., Liem, P.H., Susanti, F., Sigit, S., Nurtanto, B.D., Akhmadi, S.F., Luthfi, W., 2025b. Review on the fuel management strategy of the RSG-GAS equilibrium core. Ann Nucl Energy 213 (December 2024), 111180. https://doi.org/10.1016/j.anucene.2024.111180.

Pinem, S., Surbakti, T., Hastuti, E.P., Luthfi, W., 2025c. Transition Core from oxide to silicide fuel for Indonesian multipurpose research reactor RSG-GAS. Nucl Technol 00 (00), 1–16. https://doi.org/10.1080/00295450.2025.2472552.

Pourrostam, A., Talebi, S., Safarzadeh, O., 2021. Core analysis of accident tolerant fuel cladding for SMART reactor under normal operation and rod ejection accident using DRAGON and PARCS. Nucl Eng Technol 53 (3), 741–751. https://doi.org/10.1016/j.net.2020.08.025.

Prince, Z.M., Hanophy, J.T., Labouré, V.M., Wang, Y., Harbour, L.H., Choi, N., 2024. Neutron transport methods for multiphysics heterogeneous reactor core simulation in griffin. Ann Nucl Energy 200 (January), 110365. https://doi.org/10.1016/j.anucene.2024.110365.

PRSG, 1988. Report of The Operation of RSG-GAS Reactor First Core (Vol. 60, Issue 8).

Purdue University, 2004. OECD/NEA and U.S. NRC PWR MOX/UO2 CORE transient benchmark. https://engineering.purdue.edu/PARCS/MOX_Benchmark.

RSG-Batan, 2011. Multipurpose Reactor G.A. Siwabessy Safety Analysis Report. Rev. 10. Jakarta, Indonesia.

Sembiring, T.M., Liem, P.H., 1999. Validation of BATAN-3DIFF code on 3-D model of the IAEA 10 MWth benchmark core for partially-inserted control rods. Atom Indonesia 25 (2), 91–100 https://www.researchgate.net/publication/263593876_Validation_of_BATAN-3DIFF_code_on_3-D_model_of_the_IAEA_10_MWth_benchmark_core_for_partially-inserted_control_rods.

Sembiring, T.M., Pinem, S., 2002. Modification of Batan-2Diff code for the reactor kinetic parameters calculation. Atom Indonesia 28 (1), 1–17.

Sembiring, T.M., Tukiran, Pinem, S., Febrianto, 2001. Neutronic Design of Mixed Oxide-Silicie Cores for the Core conversion of RSG-GAS reactor. Atom Indonesia 27 (2), 95–111. ISSN 0126-1568.

Shemon, E.R., Smith, M.A., Lee, C., 2014. PROTEUS-SN Methodology Manual. Argonne National Laboratory https://publications.anl.gov/anlpubs/2014/08/79163.pdf.

Stauff, N.E., Miao, Y., Cao, Y., Mo, K., Abdelhameed, A.A.E., Ibarra, L., Matthews, C., Shemon, E.R., 2024. High-Fidelity Multiphysics Modeling of a heat pipe microreactor using BlueCrab. Nucl Sci Eng 00 (00), 1–17. https://doi.org/10.1080/00295639.2024.2375175.

Subekti, M., Isnaini, D., Hastuti, E.P., 2013. Analisis Distribusi Kecepatan Pendingin Dalam Elemen Bakar Tipe Pelat Menggunakan Metode CFD untuk Reaktor Riset RSG-GAS. Jurnal Teknologi Reaktor Nuklir 15 (2), 67–76.

Suikkanen, H., Rintala, V., Kyrki-Rajamäki, R., 2014. Development of a Coupled Multi-Physics Code System for Pebble Bed Reactor Core Modeling. Proc HTR 2014.

Vaidya, A.M., Maheshwari, N.K., Vijayan, P.K., 2010. Estimation of fuel and clad temperature of a research reactor during dry period of de-fuelling operation. Nucl Eng Des 240 (4), 842–849. https://doi.org/10.1016/j.nucengdes.2009.11.045.

Vazquez, M., Tsige-Tamirat, H., Ammirabile, L., Martin-Fuertes, F., 2012. Coupled neutronics thermal-hydraulics analysis using Monte Carlo and sub-channel codes. Nucl Eng Des 250, 403–411. https://doi.org/10.1016/j.nucengdes.2012.06.007.

Wu, X., Kozlowski, T., 2015. Coupling of system thermal-hydraulics and Monte-Carlo code: convergence criteria and quantification of correlation between statistical uncertainty and coupled error. Ann Nucl Energy 75, 377–387. https://doi.org/10.1016/j.anucene.2014.08.016.

Zhang, Q., Peng, T., Zhang, G., Liu, J., Guo, X., Gong, C., Yang, B., Fan, X., 2021. An efficient scheme for coupling OpenMC and FLUENT with adaptive load balancing. Sci Technol Nucl Install 2021. https://doi.org/10.1155/2021/5549602.